Tests of current models of intermolecular potentials against x-ray diffuse scattering in C 60

Pascale Launois, Sylvain Ravy, Roger Moret

Tests of current models of intermolecular potentials against x-ray diffuse scattering in C_{60}

Pascale Launois, Sylvain Ravy, and Roger Moret*
Laboratoire de Physique des Solides, URA 002 associée au CNRS, Bâtiment 510, Université Paris Sud, 91405 Orsay Cedex, France
(Received 25 July 1996; revised manuscript received 11 September 1996)

Diffuse scattering, which contains two-body information, is a rich source of knowledge on the interactions between the C_{60} molecules. We present a mean-field theory for calculating the diffuse scattering in the high-temperature phase of C_{60} from microscopic models of intermolecular interactions. The diffuse scattering is calculated and discussed for most of the models available to date. It is compared with single-crystal x-ray diffuse scattering data. Overall, the positions of the diffuse scattering maxima, corresponding to competing instabilities, are found to be independent of the model of interactions. This suggests that these instabilities are related to the shape of the large C_{60} molecule. No model is fully satisfactory for fitting the relative intensities of the diffuse scattering features. The best fit is obtained with the Lamoen-Michel model, which accounts also correctly for the Bragg peak intensity in the high-temperature phase. The physics of the models is discussed and some improvements are proposed. [S0163-1829(97)07804-1]

I. INTRODUCTION

C_{60} molecules have the novel shape of a truncated icosahedron,[1] with equivalent carbon sites and two types of C-C bonds (30 shorter ''double-bonds'' DB, that fuse two hexagons, and 60 longer ''single-bonds'' SB, that fuse a hexagon to a pentagon). The efficient synthesis of solid crystalline C_{60} (Ref. 2) in 1990 opened the field of solid-state investigations, including structural and dynamics studies. At atmospheric pressure, the sequence of phase transitions is as follows (see, e.g., Ref. 3 and references therein). At room temperature, the molecules adopt a face-centered-cubic lattice, with space group $Fm\bar{3}m$. They are reorienting very rapidly about their centers of gravity in this plastic phase. Moreover, diffuse scattering results give evidence of complex short-range orientational intermolecular correlations.[4–8] At $T_0 \simeq 260$ K, a first order phase transition is induced by long-range orientational order between the C_{60} molecules and the symmetry is lowered to simple cubic with four molecules per unit cell (space group $Pa\bar{3}$). There are two types of nearly degenerate equilibrium orientations for the molecules. In the more energetically favorable one, a C_{60} molecule has six pentagonal faces facing double bonds of neighboring molecules (P configuration). In the less energetically favorable one, it has six hexagonal faces facing double bonds of neighboring molecules (H configuration). The P configuration is favored as the temperature is decreased in the $Pa\bar{3}$ phase, down to a glass transition temperature $T_g \simeq 80$ K, where the populations of the two configurations are frozen. While the solid-state properties of C_{60} were investigated experimentally, improved models of intermolecular interactions were proposed, mainly based on van der Waals–type interactions (Lennard-Jones, Born-Mayer, Buckingham potentials) and on electrostatic interactions.[9–17] A good knowledge of the intermolecular interactions is important for C_{60} itself of course, but also as the prototype of the bigger fullerenes or of the doped superconducting derivatives.

The present work aims at improving our knowledge of these interactions by using the analysis of diffuse scattering as a probe for current microscopic models. The different (published) models are presented in Sec. II. Section III recalls the main characteristics of the diffuse scattering experimental data. Section IV presents the theoretical framework allowing us to calculate the diffuse scattering, while the results of the calculations are described in Sec. V. Detailed comparisons between experimental and calculated diffuse scatterings are presented. Calculation results are discussed in Sec. VI. One of the models[15] fits the experimental data better than the others although it is not fully satisfactory. Possible further improvements are discussed.

II. CURRENT MODELS OF INTERMOLECULAR POTENTIALS IN C_{60}

The first intermolecular potentials for C_{60} were atom-atom potentials derived from those already known for graphite.[9,10] Such choices appear reasonable because the minimum distance between carbon atoms of neighboring molecules is comparable with the interlayer spacing in graphite. Nevertheless, these models predicted orthorhombic[9] or tetragonal[10] low temperature phases instead of the observed simple cubic one. Hence, improved models of potentials with additional van der Waals centers of interactions and/or with electrostatic interactions between charges on the molecules were proposed. For an atom-atom 12-6 Lennard-Jones potential (vdW model[10,18]), the tetragonal structure was characterized by a crossing of DB's at minimum separation. To avoid this, Sprik, Cheng, and Klein[11] supplemented the 60 atomic 12-6 sites C with 30 12-6 sites located at the centers of the DB's (SCK1 model). This was sufficient to stabilize the $Pa\bar{3}$ phase at low temperature. In order to raise the transition temperature closer to the experimental one, they improved their model assigning a negative charge q_D to the centers of the DB's, and the compensating charges (for the molecule neutrality) $q_C = -q_D/2$ to the carbon atoms (SCK2 model). Independently, Lu, Li, and Martin[12] improved the vdW model by assigning an effective charge q_S to the centers of SB's, and the compensating charges $(-2q_S)$ to the DB centers (LLM model). They also

TABLE I. Models of intermolecular potential, after Refs. 11,12,15, and 17; e is the absolute value of the charge of the electron.

Model	Form of the potential	Interaction centers	Parameter values
vdW	$D\times[(\sigma/r)^{12}$ $-2(\sigma/r)^6]$	carbon atoms (C)	$D=34.5$ K $\sigma=3.8$ Å
SCK1	$D\times[(\sigma_{x-x'}/r)^{12}$ $-2(\sigma_{x-x'}/r)^6]$	$x,x'=$C, DB centers	$D=12$ K, $\sigma_{\mathrm{C\text{-}C}}=3.8$ Å, $\sigma_{\mathrm{C\text{-}DB}}=3.93$ Å, $\sigma_{\mathrm{DB\text{-}DB}}=4.04$ Å
SCK2	SCK1 $+q_x q_{x'}/r$	$x,x'=$C, DB centers	$D=15$ K, same σ's as for SCK1, $q_C=0.175e$, $q_{\mathrm{DB}}=-0.35e$
LLM	$\mathrm{vdW}_{\mathrm{C\text{-}C}}$ $+q_x q_{x'}/r$	$x,x'=$ DB and SB centers	same D and σ's as for the vdW model, $q_{\mathrm{SB}}=0.27e$, $q_{\mathrm{DB}}=-0.54e$
LM	$C_1^{x-x'}\exp(-C_2^{x-x'}r)$ $-B_{x-x'}/r^6$	$x,x'=$C, 3 centers on DB's ($\mathrm{DB}_i, i=1-3$), 1 center on SB's	$B_{\mathrm{C\text{-}C}}=305\,421$ K Å^6, others $B=0$, $C_1^{\mathrm{C\text{-}C}}=1.2, C_1^{\mathrm{DB}_i-\mathrm{DB}_j}=0.072$, $C_1^{\mathrm{C\text{-}DB}_i}=0.1, C_1^{\mathrm{SB,C\text{-}SB}}=0.22$ $C_1^{\mathrm{DB}_i-\mathrm{SB}}=0$, in units 374 530 00 K $C_2^{\mathrm{C\text{-}C}}=3.6, C_2^{\mathrm{DB}_i-\mathrm{DB}_j}=3.2$, $C_2^{\mathrm{C\text{-}DB}_i}=3.4, C_2^{\mathrm{SB,C\text{-}SB}}=3.6$ Å^{-1}
PC	$C_1\exp(-C_2 r)-B/r^6$ $+q_x q_{x'}/r$	$x,x'=$C, charges inside (1) and outside (2) of the molecule	C-C: $B=155\,000$ K Å^6, $C_1=209\,814\,23$ K, $C_2=3.532$ Å^{-1}, $q_1=q_2=-0.27e, q_{\mathrm{C}}=0.27e$

succeeded in stabilizing the $Pa\bar{3}$ phase at low temperature (an interesting discussion of the C_{60} phase diagram for models derived from the SCK's and LLM ones, within the frame of a mean-field theory similar to that used here, is given by Heid[18]). Burgos, Halac, and Bonadeo[13] introduced another charge model, placing 30 charges q_D on the DB's and 12 charges $[-5/2(q_D)]$ at the pentagon centers. However, Yildirim, Harris, Erwin, and Pederson[19] determined the charge distribution of the C_{60} molecule from *ab initio* calculations, and they found that the charges carried by pentagons and hexagons are too different from each other for both SCK2 and LLM models. The pentagon and hexagon charges differ too much also in the model of Burgos *et al.*, so that it has not been retained for calculating the diffuse scattering; a further motivation will be given in Sec. VI B 3.

While the SCK's and LLM models were essentially elaborated to account for the C_{60} low temperature phase, other models were introduced in the light of more recent experimental results, namely from crystallographic and inelastic neutron scattering studies. First, precise measurements of the Bragg reflections enabled the determination of the crystal-field energy, which acts on a molecule due to its neighbors, in the high temperature $Fm\bar{3}m$ phase. Lamoen and Michel used these data to adjust the parameters of a model (LM model)[14,15] in which they considered Born-Mayer repulsions and van der Waals attractions between carbon atoms but also between other interaction centers along the DB's and at the centers of the SB's. Note that a slightly different version of this model is now proposed by Michel and Copley,[16] but we will not focus on this most recent one as it gives very similar results and leads to the same conclusions. Second, in order to fit the phonon dispersion curves measured by inelastic neutron scattering, Pintschovius and Chaplot[17] introduced a new bond charge model (PC model), with a charge q at the carbon atom position, and where the DB charge $(-2q)$ is split in the radial direction in two charges $(-q)$ inwards and outwards of the surface of the molecule.

The parameters of the interaction potentials to be discussed in the following are summarized in Table I.

III. C_{60} DIFFUSE SCATTERING OBSERVATIONS AT ROOM TEMPERATURE

While Bragg diffraction provides one-body information, diffuse scattering, i.e., the weak intensity distributed between the Bragg peaks, contains two-body information. It is thus a rich source of knowledge on the correlations between atoms or molecules (see for instance the recent reviews of Welberry and Butler[20]).

Diffuse scattering in C_{60} at room temperature was first measured by powder neutron scattering, in the form of two broad halos at wave vectors of about 3.3 and 5.3 Å^{-1}. These halos could be well accounted for by assuming rotational diffusion of the molecules with no correlations.[21] However, scattering from powders only gives limited information on correlations because of the angular average. C_{60} single crystals of good quality became available in 1992, allowing the first single-crystal diffuse scattering investigation to be made,[4] using x rays and the monochromatic fixed-film, fixed-crystal photographic technique. Rich azimuthal modulations of the halos were found, evidencing intermolecular correlations at room temperature. Subsequently, we performed an extensive study of the diffuse scattering in the first

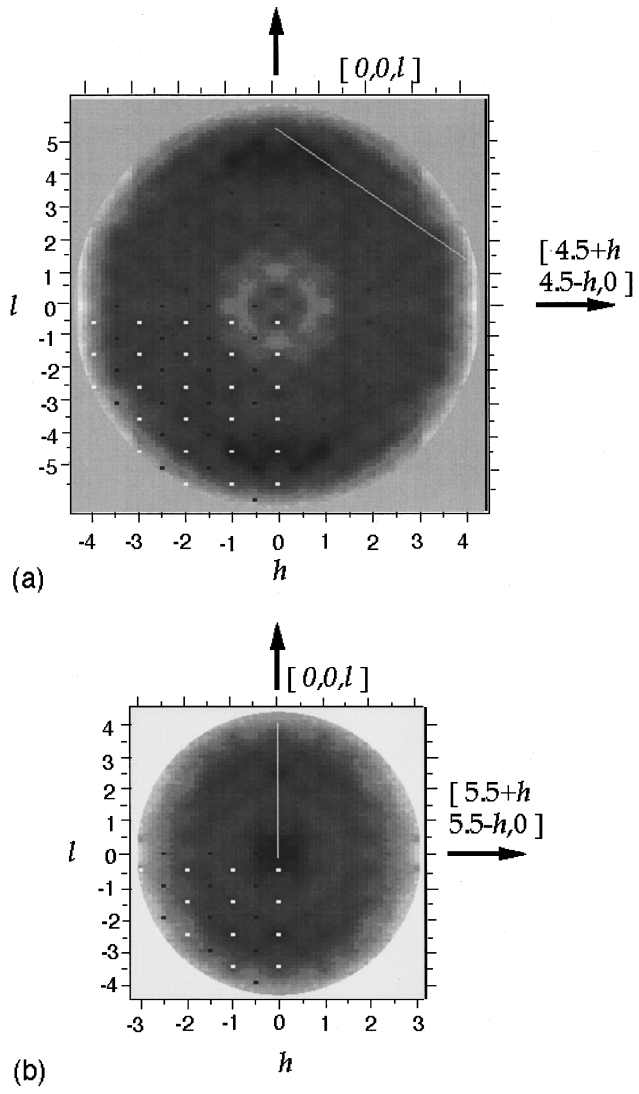

FIG. 1. X-ray diffraction patterns for the planes (a) $h+k=9$, (b) $h+k=11$ (data are corrected for absorption and polarization effects). Large diffuse intensities correspond to dark areas. The black and white dots shown in one quadrant pinpoint to the points X and L, respectively. The solid lines indicate scan directions in Fig. 2.

halo at room temperature,[6] using Cu $K\alpha$ x rays and a three-circle diffractometer that enabled quantitative 3D data collection. The results have been described in recent papers[6,22,23] and their main features are summarized below using characteristic 2D sections and linear scans of the modulated diffuse scattering intensity. The diffuse scattering modulations can be analyzed in terms of maxima of scattering at the points $X=(1,0,0)$, $L=(\frac{1}{2},\frac{1}{2},\frac{1}{2})$, and $\Gamma=(0,0,0)$ of the Brillouin zone (BZ), plus some extra scattering which does not present a maximum at a special point of the Brillouin zone. X and L scatterings are visible in the $h+k=9$ and $h+k=11$ planes (Fig. 1), where the distribution of maxima in staggered rows of points X and L is clearly observed; this can also be seen in the linear scan shown in Fig. 2(a). Moreover, at the center of the plane $h+k=11$, the diffuse scattering takes the form of a thick ''H,'' which is among the most intense extra-scattering features of the whole diffuse halo [see also the linear scan in Fig. 2(b)]. The Γ scattering is evidenced in the linear scan in Fig. 2(c). One sees in Figs.1 and 2 that X,L,Γ and extra-scattering intensities are of the same order of magnitude. They also correspond to similar correlation lengths of about 5 Å (for the ''H'' scattering, this is measured perpendicularly to the plane $h+k=11$).[6] We mention that the X-point scattering was studied by Blaschko *et al.*,[5] that the rich scattering features in C_{60} have also been observed by Wochner *et al.*,[8] and that the existence of both X and L point maxima has been deduced independently from single-crystal neutron diffraction experiments by Pintschovius *et al.*, with, however, larger correlation lengths (up to 40 Å).[7] The difference between x-ray and neutron correlation lengths may be attributed (i) to the chosen form of the correlation functions, namely, particle size broadening function in Ref. 7 and Ornstein-Zernike correlation function in Ref. 6, which induces a factor of ~ 3 between the corresponding correlation lengths (we have chosen the Ornstein-Zernike form, which is appropriate in the case of pretransitional fluctuations); (ii) to energy resolution effects [in neutron experiments, the 40 Å value corresponds to the small energy window, while a smaller value is measured for a broader window (Fig. 1 in Ref. 7)].

If X-point scattering had been observed alone, it would have been interpreted as pretransitional diffuse scattering, since points X correspond to positions of the superstructure peaks in the low temperature phase $Pa\bar{3}$. However, the observed complex diffuse scattering points towards much more complicated local ordering and reveals the existence of competing fluctuations in C_{60}.[6,16,18,22,24] To clarify this point, especially in terms of models of intermolecular potentials, elaborated calculations or simulations are necessary. Monte Carlo or molecular dynamics simulations can be performed, allowing one to find the density-density correlation functions in direct space and to calculate diffuse scattering patterns in reciprocal space. The main drawback of these approaches is that they imply time-consuming calculations, and thus limits on sample sizes. Molecular dynamics simulations based on the PC model have been performed by Pintschovius, Chaplot, Roth, and Heger.[7] On the other hand, the statistical average of the correlation functions can be calculated analytically, within the framework of a mean-field approximation. This method allows one to compute the diffuse scattering more rapidly.[25] But contrary to Monte Carlo or molecular dynamics techniques, it does not easily allow direct space visualization. However, we have chosen this method for its reasonable computation times, which permits the comparison of different models of intermolecular interactions. Our first computations, for the vdW and SCK1 models, were presented in Ref. 22; similar calculations for the modified LM model have been done by Michel and Copley in Ref. 16.

IV. THEORETICAL FRAMEWORK

In this section, we first recall the concepts underlying the derivation of the scattering intensities, using the formalism of the symmetry-adapted functions. This powerful formalism has been applied to several cases of orientationally disordered solids[26] and to C_{60} in particular.[3,6,14–16,18,22,24,28–32] It leads to an expression of the diffuse intensity in terms of orientational pair correlation functions.[3,6,28] Then, using a mean-field approximation, we evaluate these pair correlation

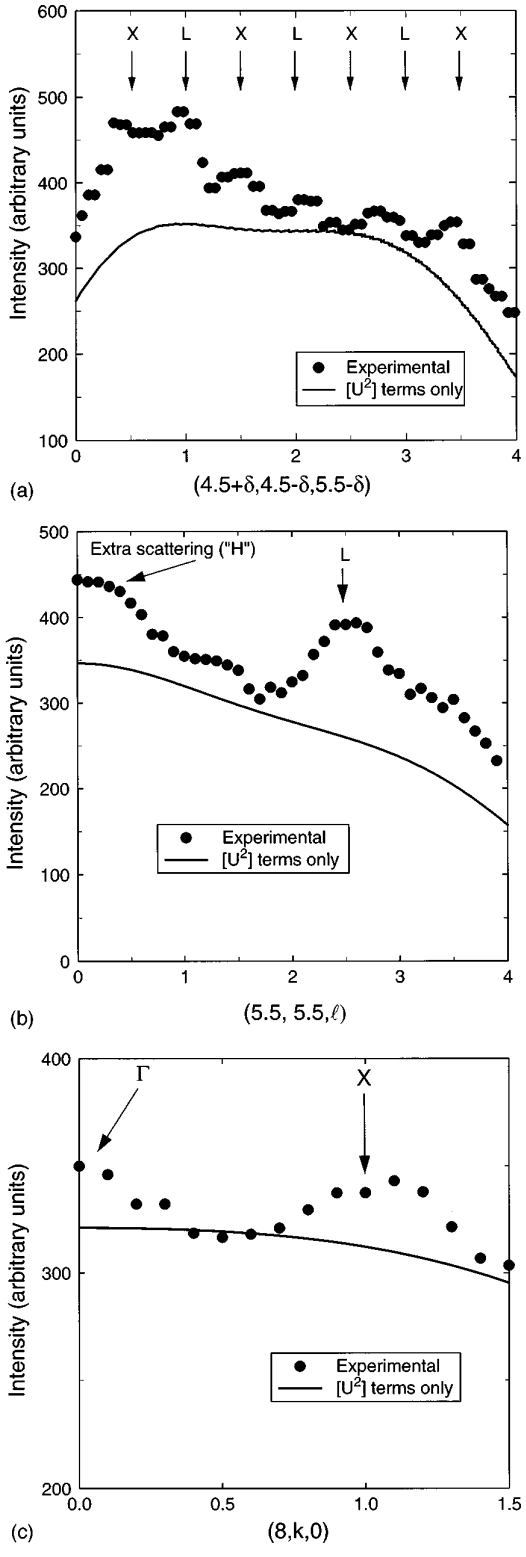

FIG. 2. X-ray diffraction intensity (a) along a selected line of the plane $h+k=9$, from (4.5,4.5,5.5) to (8.5,0.5,1.5), (b) along a selected line of the plane $h+k=11$, from (5.5,5.5,0) to (5.5,5.5,4), and (c) in the [8,k,0] direction; the (8,0,0) Bragg peak contribution is substracted [it is weak due to an accidental pseudoextinction: this allows one to observe the Γ point diffuse scattering at an $Fm\bar{3}m$ Bragg peak position (Ref. 6)]. Data are corrected for absorption and polarization effects. A constant background (200 counts) has been substracted. The solid lines result from calculations with the experimental $[U^2]$ term only, as explained in Sec. VI B 2.

functions in terms of the intermolecular interactions.[22] The theoretical formulation is presented below. Special emphasis is put on the mean-field theory for evaluating the pair correlation functions, which was not yet developed in detail in previous work.[22]

The angular part of the atomic density of a molecule reads[3,6,28]

$$\rho(\Omega)=\sum_{\nu=1}^{60}\delta(\Omega-\Omega_\nu)=\sum_{l=0}^{\infty}g_l S_l(R_\omega^{-1}\Omega), \tag{1}$$

where Ω stands for the polar angles (θ,φ) with respect to the fourfold cubic axes. The first sum runs over the sixty atoms ν of the molecule. The second sum is a development over angular momentum components l. The functions $S_l(\Omega)$ are the icosahedral harmonics, available from Refs. 27 and 33. The first harmonics are $l=0,6,10,12,16$, and 18, the associated molecular form factors being $g_0\simeq 16.9$, $g_6\simeq 2.6$, $g_{10}\simeq 19.4$, $g_{12}\simeq 7.9$, $g_{16}\simeq -17.9$, and $g_{18}\simeq 38.2$. The orientation of the molecule with respect to its standard orientation, represented in Fig. 6(a) in Ref. 6, is determined by the three Eulerian angle set ω (rotation R_ω).

The icosahedral harmonics S_l can be expressed in terms of the cubic symmetry-adapted functions S_l^τ, given in Ref. 34 up to $l=12$,

$$S_l(R_\omega^{-1}\Omega)=\sum_\tau U_l^\tau(\omega)S_l^\tau(\Omega). \tag{2}$$

The index τ stands for the combination (Γ,μ,i), where Γ is an irreducible representation of the cubic group $m\bar{3}m$, μ distinguishes between representations that occur more than once within a given l manifold, and i labels rows of the representation. The functions $U_l^\tau(\omega)$ are named rotators. They are symmetry-adapted linear combinations of the Wigner rotation matrix elements, but they can also be directly calculated from the cubic symmetry-adapted functions by

$$U_l^\tau(\omega)=\frac{1}{g_l}\sum_{\nu=1}^{60}S_l^\tau(\Omega_\nu). \tag{3}$$

The x-ray C_{60} structure factor, deduced from the Fourier transform of $\rho(\Omega)$, reads[3,28]

$$F(\mathbf{Q})=4\pi f_C(Q)\sum_l\sum_\tau i^l g_l j_l(QR)S_l^\tau(\Omega_\mathbf{Q})U_l^\tau(\omega), \tag{4}$$

where $\mathbf{Q}$ is the scattering wave vector of modulus Q, j_l is the spherical Bessel function of order l, and R is the C_{60} molecule radius. The contribution of bond electrons is neglected in this equation where $f_C(Q)$ is simply the carbon atomic scattering factor; this is justified by the agreement between analyses of neutron and x-ray crystallographic data, with this approximation for x-ray.[29] The scattering consists of Bragg peaks at the reciprocal lattice vectors $\mathbf{G}$, and of diffuse scattering at wave vectors $\mathbf{Q}=\mathbf{G}+\mathbf{q}$, where $\mathbf{q}$ is the wave vector inside the first BZ. From Eq. (4), and following the calculations in Ref. 28, the Bragg and diffuse scattering intensities in the high temperature phase $Fm\bar{3}m$ are[6]

$$I_B(\mathbf{Q}=\mathbf{G}) \propto 16\pi^2 N^2 f_C^2 \Big| \sum_{l=0}^{\infty} \sum_{\tau=(A_{1g},\mu)} i^l g_l j_l(QR) S_l^{\tau}(\Omega_{\mathbf{Q}}) \times \langle U_l^{\tau}(\omega) \rangle \Big|^2, \tag{5}$$

$$I_D(\mathbf{Q}=\mathbf{G}+\mathbf{q};\mathbf{q}\neq 0) \propto 16\pi^2 N f_C^2 \sum_{l,l'\geq 6}^{\infty} \sum_{\tau,\tau'} i^{l-l'} g_l g_{l'} j_l(QR) j_{l'}(QR) \times S_l^{\tau}(\Omega_{\mathbf{Q}}) S_{l'}^{\tau'}(\Omega_{\mathbf{Q}}) \langle U_l^{\tau}(\mathbf{q}) U_{l'}^{\tau'}(-\mathbf{q}) \rangle, \tag{6}$$

where N is the total number of molecules in the crystal and where the Fourier transforms of the rotator site values are defined by

$$U_l^{\tau}(\mathbf{q}) = \frac{1}{\sqrt{N}} \sum_n U_l^{\tau}(\omega_n) \exp(i\mathbf{q}\cdot\mathbf{X}_n). \tag{7}$$

The representations involved in the expression of Bragg peak intensities are the identity—A_{1g}—representations, the only ones for which the rotator mean values are nonzero. Moreover, as expected, the diffuse scattering intensity in Eq. (6) is expressed in terms of orientation-orientation pair correlation functions or, more precisely, in terms of the pair correlation functions of the Fourier transforms of the rotators. One now needs to evaluate these pair correlation functions for the different models of intermolecular interactions proposed for C_{60}. This is done within the framework of a mean-field approximation, justified by the rather short extent of the correlations [$\sim$5 Å, (Ref. 6)] compared to the range of the interactions ($\sim$10 Å, the nearest-neighbor distance). Due to the first order character of the $Fm\bar{3}m$-$Pa\bar{3}$ phase transition, the room temperature diffuse scattering is not critical in nature.

The orientational energy in the high temperature phase $Fm\bar{3}m$ is

$$E = \frac{1}{2} \sum_{i,j} V(\omega_i, \omega_j) = \frac{1}{2} \sum_{i,j} \sum_{l,l',\tau,\tau'} J_{l,l'}^{\tau,\tau'}(i,j) U_l^{\tau}(\omega_i) U_{l'}^{\tau'}(\omega_j), \tag{8}$$

where i and j label molecules in the crystal. The interaction matrix element $J_{l,l'}^{\tau,\tau'}$ reads

$$J_{l,l'}^{\tau,\tau'}(i,j) = \sum_{I,J} g_l^I g_{l'}^J v_{ll'\tau\tau'}^{ijIJ}. \tag{9}$$

The form factors $g_l^I, g_{l'}^J$ are calculated for the distribution of the interaction centers I and J (such as van der Waals or electrostatic interaction centers), and the interaction terms $v_{ll'\tau\tau'}^{ijIJ}$ can be expressed as[14,15,27,28]

$$v_{ll'\tau\tau'}^{ijIJ} = \int \int d\Omega_i d\Omega_j v^{ijIJ}(\mathbf{r}_1, \mathbf{r}_2) S_l^{\tau}(\Omega_i) S_{l'}^{\tau'}(\Omega_j), \tag{10}$$

where $v^{ijIJ}(\mathbf{r}_1, \mathbf{r}_2)$ is the microscopic interaction energy between interaction centers of types I and J at the positions $\mathbf{r}_1$ and $\mathbf{r}_2$, located on the molecules labeled i and j. We underline that Eq. (10) is used as such when interaction center densities do not overlap between neighboring molecules, to avoid infinite values in the integral. This is the case for the models studied in this paper (Table I). For overlapping densities, a special treatment is needed.[24]

The mean-field approximation consists in expressing the orientational energy in Eq. (8) in terms of the mean values of the rotators and of the fluctuations around these mean values, and in neglecting the second order fluctuations,

$$E \simeq -\frac{1}{2} \sum_{i,j} \sum_{l,l',\tau,\tau'} J_{l,l'}^{\tau,\tau'}(i,j) \langle U_l^{\tau}(\omega_i) \rangle \langle U_{l'}^{\tau'}(\omega_j) \rangle + \sum_{i,j} \sum_{l,l',\tau,\tau'} J_{l,l'}^{\tau,\tau'}(i,j) U_l^{\tau}(\omega_i) \langle U_{l'}^{\tau'}(\omega_j) \rangle. \tag{11}$$

Since the terms containing only mean values of rotators, or the $l=0$ rotator ($U_0=1$), would cancel out in the following mean-field equations, we keep now an expression of the mean-field energy up to these constant terms; the total mean-field energy is the sum of the mean-field energies of each individual molecule i,

$$E_{\mathrm{MF}}(\omega_i) = \sum_{l\geq 6,\tau} e_{l,\mathrm{MF}}^{\tau}(i) U_l^{\tau}(\omega_i), \tag{12}$$

with

$$e_{l,\mathrm{MF}}^{\tau}(i) = \sum_j \sum_{l'\geq 0,\tau'} J_{l,l'}^{\tau,\tau'}(i,j) \langle U_{l'}^{\tau'}(\omega_j) \rangle. \tag{13}$$

Note that in the high temperature phase $Fm\bar{3}m$, and in the absence of an external field, (i) all molecules are equivalent [$e_{l,\mathrm{MF}}^{\tau}(i) \equiv e_{l,\mathrm{MF}}^{\tau}$], and (ii) only the identity representations remain: $\tau=\tau'=A_{1g,\mu}$. For $l\leq 12$ (multipole expansion will be limited to $l=12$ in the following), there are four $e_{l,\mathrm{MF}}^{\tau=A_{1g},\mu}$ terms: one for $l=6$, one for $l=10$, and two for $l=12$, because there are two A_{1g} representations belonging to the $l=12$ manifold ($\mu=1,2$). The mean values of the rotators $\langle U_l^{\tau}(\omega_i) \rangle$ are obtained by solving the self-consistent mean-field equations

$$\langle U_l^{\tau}(\omega_i) \rangle = \frac{\int d\omega_i U_l^{\tau}(\omega_i) \exp(-E_{\mathrm{MF}}/(kT))}{\int d\omega_i \exp(-E_{\mathrm{MF}}/(kT))}. \tag{14}$$

Introducing the fields conjugated to the rotators, the mean-field energy becomes

$$E_{\mathrm{MF}} = \sum_i \sum_{l\geq 6,\tau} [e_{l,\mathrm{MF}}^{\tau}(i) - h_l^{\tau}(i)] U_l^{\tau}(\omega_i). \tag{15}$$

The zero-field susceptibility matrix has components defined by

$$\chi_{l,l'}^{\tau,\tau'}(i,j) = \left(\frac{\partial \langle U_l^{\tau}(\omega_i) \rangle}{\partial h_{l'}^{\tau'}(j)} \right)_{h_{l'}^{\tau'}(j)\to 0}. \tag{16}$$

Using Eqs. (14) and (15), Eq. (16) becomes

$$kT\chi_{l,l'}^{\tau,\tau'}(i,j)+\left(\sum_k \sum_{l'',l''',\tau'',\tau'''} J_{l',l'''}^{\tau',\tau'''}(i,k)\chi_{l''',l'}^{\tau''',\tau'}(k,j) - \delta_{l',l'';\tau',\tau'';i,j}\right)[U^2]_{l,l''}^{\tau,\tau''}=0, \quad (17)$$

where δ is the Kronecker symbol (equal to zero if $l'\neq l''$ or $\tau'\neq\tau''$ or $i\neq j$), and where the matrix $[U^2]$ is defined by

$$[U^2]_{l,l'}^{\tau,\tau'}=\langle U_l^{\tau}(\omega)U_{l'}^{\tau'}(\omega)\rangle-\langle U_l^{\tau}(\omega)\rangle\langle U_{l'}^{\tau'}(\omega)\rangle. \quad (18)$$

The brackets indicate averages over the mean-field energy as in Eq. (14). Introducing the Fourier transformed matrices $[\chi(\mathbf{q})]$ and $[J(\mathbf{q})]$ given by

$$[\chi(\mathbf{q})]_{l,l'}^{\tau,\tau'}=\sum_{\mathbf{r}} \chi_{l,l'}^{\tau,\tau'}(\mathbf{r})\exp(i\mathbf{q}\cdot\mathbf{r}),$$

$$[J(\mathbf{q})]_{l,l'}^{\tau,\tau'}=\sum_{\mathbf{r}} J_{l,l'}^{\tau,\tau'}(\mathbf{r})\exp(i\mathbf{q}\cdot\mathbf{r}), \quad (19)$$

$\mathbf{r}$ corresponding to (i,j) in Eqs. (9) and (16), we obtain

$$[\chi(\mathbf{q})]=[kT[U^2]^{-1}+[J(\mathbf{q})]]^{-1}. \quad (20)$$

The pair correlation terms in Eq. (6) are related to the susceptibility by the fluctuation-dissipation theorem

$$\langle U_l^{\tau}(\mathbf{q})U_{l'}^{\tau'}(-\mathbf{q})\rangle=kT\chi_{l,l'}^{\tau,\tau'}(\mathbf{q}). \quad (21)$$

From Eqs. (6), (20), and (21), we can express the diffuse scattering intensity at any point in reciprocal space,

$$I_D(\mathbf{Q}=\mathbf{G}+\mathbf{q};\mathbf{q}\neq 0) \propto f_C^2 kT \sum_{l,l'\geqslant 6}^{\infty} \sum_{\tau,\tau'} i^{l-l'} g_l g_{l'} j_l(QR) j_{l'}(QR) \times S_l^{\tau}(\Omega_{\mathbf{Q}}) S_{l'}^{\tau'}(\Omega_{\mathbf{Q}}) ([kT[U^2]^{-1}+[J(\mathbf{q})]]^{-1})_{l,l'}^{\tau,\tau'}. \quad (22)$$

We can now evaluate the diffuse scattering intensity for different models of intermolecular interactions. The successive steps of the calculation are as follows. For a given model of intermolecular potential, we calculate all the interaction terms from Eq. (10) to get the $[J(\mathbf{q})]$ matrix. The self-consistent equations (14) are solved to derive the mean-field energy $E_{\mathrm{MF}}(\omega_i)$ [Eqs. (12) and (13)] and then $[U^2]$. Calculations are performed for the first-neighbor interaction terms belonging to *all* representations up to $l=12$, that is, for 59×59 matrices.

To end this section, let us discuss the different levels of approximation which can be considered when evaluating I_D [Eq. (22)], especially with respect to the multipole expansion. The radial component of the diffuse scattering intensity is given by the spherical Bessel functions $j_l(QR)$ weighted by the molecular form factors g_l. These are the only contributing terms for isotropic and uncorrelated molecular rotations. In that case, Eq. (22) reduces to

$$I_D(\mathbf{Q})\propto f_C^2 \sum_{l=6}^{\infty} (g_l j_l(QR))^2. \quad (23)$$

Our diffuse scattering experiments[6] were performed in the first diffuse halo located at $Q_1\simeq 3.3$ Å^{-1}, for 2.64 Å$^{-1}\leqslant Q\leqslant 3.96$ Å^{-1}. We will thus restrict our calculations to this halo. The first maximum of $j_l(QR)$ occurring for $Q_{\max}\simeq l/R$ and j_l intensity strongly decreasing for $Q<Q_{\max}$,[3] the radial component of the first halo will be described by only a few spherical Bessel functions. It is dominated by the $l=10$ term in Eq. (23), and it can be entirely described by the $l=6$, 10, and 12 terms. However, it may be necessary to calculate the $[J]$ and $[U^2]$ matrices to higher multipolar order, if for instance the coupling between the $l\leqslant 12$ terms and some $l'>12$ terms was important. The interaction strength $J_{l,l'}^{\tau,\tau'}(i,j)$ between interaction centers of types I and J, belonging to molecules i and j, respectively, scales approximately as

$$g_l^I g_{l'}^J \left(\frac{r_I+r_J}{d_{ij}}\right)^{l+l'}, \quad (24)$$

where r_I and r_J are the radii of the spheres on which interaction centers I and J are located, and where d_{ij} is the distance between molecule i and j centers of mass;[35] this allows one to restrict calculations up to a maximum value $l_{\max}$ in the multipole expansion and over a given distance between neighbors. Evaluating (24) for the various types of interaction centers in Table I, we conclude that $l\leqslant 12-l'>12$ couplings can be neglected, because the $l-l'$ or the $l'-l'$ terms are sufficiently small (it is true for $l>0$, i.e., for the $[J(\mathbf{q})]$ matrix in Eq. (22), but also for the $J_{l=0,l'}$ terms in Eq. (13)). This is true for all the models of interactions studied in this paper, even for the PC one, where greater values of $([r_I+r_J]/d_{ij})$ are obtained for the charges outside the molecules. Hence, to summarize, diffuse scattering calculations in the first halo can be restricted to $l\leqslant 12$. We need to consider the interaction terms for *all* the representations with $l\leqslant 12$ (this will be detailed in Sec. VI A). Finally, evaluation of Eq. (24) for nearest neighbors, next-nearest neighbors, etc., shows that nearest neighbor interactions are clearly dominant, so that our calculations are restricted to nearest neighbors.

V. DIFFUSE SCATTERING CALCULATIONS FOR CURRENT MODELS OF INTERMOLECULAR POTENTIALS

A. Mean-field temperature scales

The previous mean-field approach predicts a second order phase transition when the susceptibility $[\chi(\mathbf{q})]$ diverges, whereas the $Fm\bar{3}m-Pa\bar{3}$ phase transition occurring at $T_0\simeq 260$ K is in fact a first order one. This approximation will give valuable results concerning the fluctuations in the high temperature phase if the temperature at which calculations are performed is sufficiently far above the second order (calculated) transition temperature T_C, so that the fluctuations extend over the same distances as observed (~ 5 Å). For this reason, and because we use a mean-field approximation (see below), the absolute temperatures are unphysical. Hence, for simplicity, the lattice expansion with temperature is not taken into account: all calculations are performed using the room temperature lattice parameter.

TABLE II. Second order transition temperatures and temperatures at which diffuse scattering calculations are performed for the different models of intermolecular potentials.

Model	Second order transition temperature	Calculation temperature
vdW	140 K$<T_c<$150 K	300 K
SCK1	130 K$<T_c<$140 K	300 K
SCK2	320 K$<T_c<$330 K	500 K
LLM	610 K$<T_c<$620 K	800 K
LM	320 K$<T_c<$330 K	500 K
PC	1140 K$<T_c<$1150 K	1600 K

To evaluate the transition temperature for each model of interactions (Table I), we solved the mean-field equations (14) at different temperatures T, and then studied the susceptibility—Eq. (20)—eigenvalues: if they are all positive, $T>T_c$, and when an eigenvalue becomes negative, $T<T_c$; the second order phase transition corresponds to a divergence of an eigenvalue of the susceptibility. The second order transition temperatures determined for the vdW, SCK1, SCK2, LLM, LM, and PC models are reported in Table II. As usual the transition temperatures calculated within a mean-field theory are overestimated, because not all fluctuations are taken into account. For instance, the mean-field second order transition temperatures are $T_c \simeq 135$ K and $T_c \simeq 1145$ K for the SCK1 and PC models, and mean-field first order transition temperatures—which could be obtained developing the free energy up to fourth order terms—are even higher, whereas molecular dynamic calculations[11,7] give transition temperatures of about 110 K and lower than 900 K, respectively. The mean-field second order transition temperatures are reference values for the diffuse scattering calculations, which must be done sufficiently far above. To determine the calculation temperature for each model, we calculated the diffuse scattering at different temperatures above the transition, and then selected the most appropriate temperature through a comparison with the experimental data; the calculation temperatures chosen for each model are reported in Table II. This is illustrated for the LM model by Figs. 3(a) and 3(b), where the diffuse scattering planes $h+k=9$ calculated at 500 K and 350 K are reported: comparison with experiment in Fig. 1(a) shows that $T=350$ K is much too close to the transition temperature (some diffuse features are too sharp).

B. Diffuse scattering calculations

We now present calculations of the diffuse scattering for the vdW, SCK1, SCK2, LLM, PC, and LM models for the temperatures indicated in Table II. Our earlier results for the vdW or the SCK1 models have already been presented in Ref. 22. Diffuse scattering calculations within a mean-field theory are also performed by Michel and Copley, for a slightly modified LM model,[16] which leads to results similar to those of Fig. 3(b).

The calculated diffuse scattering planes $h+k=9$ and $h+k=11$ are displayed in Figs. 3(a) and 3(c), for the LM model. They were presented in Figs. 1 and 2(b) in Ref. 22 for the vdW model. These models correspond, respectively, to the most elaborated and to the simplest distributions of van der Waals–type interaction centers. In both cases, the X and L point scatterings are clearly observed, together with the ''H-shaped'' extra scattering (compare with Fig. 1). Similar observations were made for the SCK1 model, as shown in Ref. 22 also. Actually this is the case for all models in Table I, including those with additional electrostatic charges, as is illustrated in the linear scans within the planes $h+k=9$ and $h+k=11$, in Figs. 4(a) and 4(b). Moreover, all models produce diffuse maxima at Γ points. The (8,0,0) Γ position is a diffuse scattering maximum for the vdW, LLM, LM, and PC models; this is evidenced in Fig. 4(c). It corresponds to a minimum for the SCK1 and SCK2 models, but this is an accidental depletion: diffuse scattering patterns calculated for the SCK models generally present Γ point maxima. Thus, the existence of a complex diffuse scattering in C_{60}, with X,L,Γ point and extra scatterings, is predicted by all models of intermolecular interactions in Table I (see also Refs. 7,22, and 23). This can be attributed to the high symmetry and the numerous atoms of the C_{60} molecule which create competing pretransitional fluctuations, as further developed in Sec. VI A.

Examination of Figs. 4(a)–4(c) shows that the diffuse scatterings calculated for the various models of interactions differ by the relative intensities of the X,L,Γ point and extra scatterings. Comparing with the observed intensities we find that, depending on the region of reciprocal space considered, opposite conclusions can be reached. For instance, the intensity calculated for the SCK1 model is the best in Fig. 4(a), but it is the worst in Figs. 4(b) and 4(c). Similarly, the intensity calculated for the vdW model fits correctly the measured one in Fig. 4(c), but is the worst in Fig. 4(a). The PC model, which accounted fairly well for the diffuse scattering in a particular region,[7] fails to reproduce its distribution in other regions of reciprocal space, as is evidenced in Fig. 4(a), for instance. These results prove that it is necessary to analyze the diffuse scattering in extended regions of reciprocal space.[22] Accordingly, one finds that the model for which the diffuse scattering distribution is best simulated is the LM model. Indeed, it is the only one for which the experiments are at least correctly reproduced in Figs. 4(a), 4(b), and 4(c) altogether [compare also Figs. 3(a) and 3(c) with Figs. 1(a) and 1(b)]. The results of the diffuse scattering calculations for the LM model are discussed in more details in Secs. VI B and VI C.

It is worth pointing out that the description of the diffuse scattering intensity distribution in terms of X,L,Γ and extra scatterings should be taken with caution because other types of analyses may be equally or even more appropriate. For instance some diffuse streaks can be identified in the

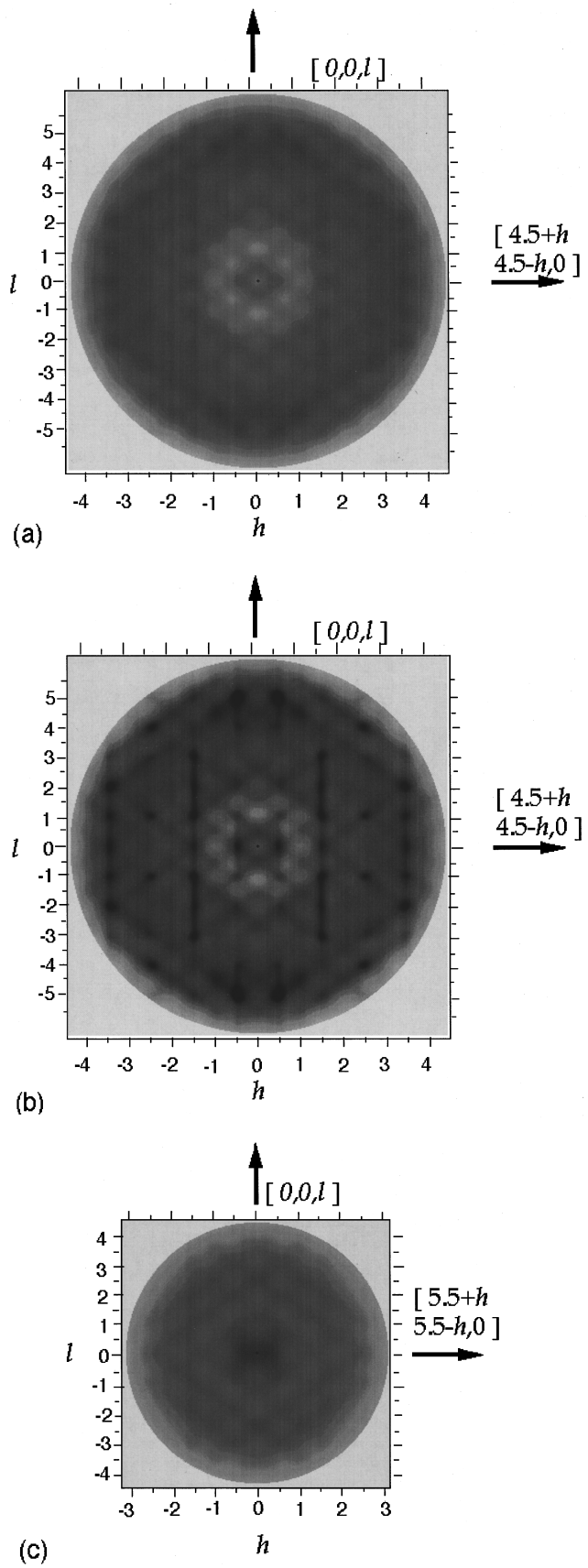

FIG. 3. Calculated x-ray diffuse scattering patterns for the LM model: (a) plane $h+k=9$, $T=500$ K, (b) plane $h+k=9$, $T=350$ K, and (c) plane $h+k=11$, $T=500$ K. Large diffuse intensities correspond to dark areas.

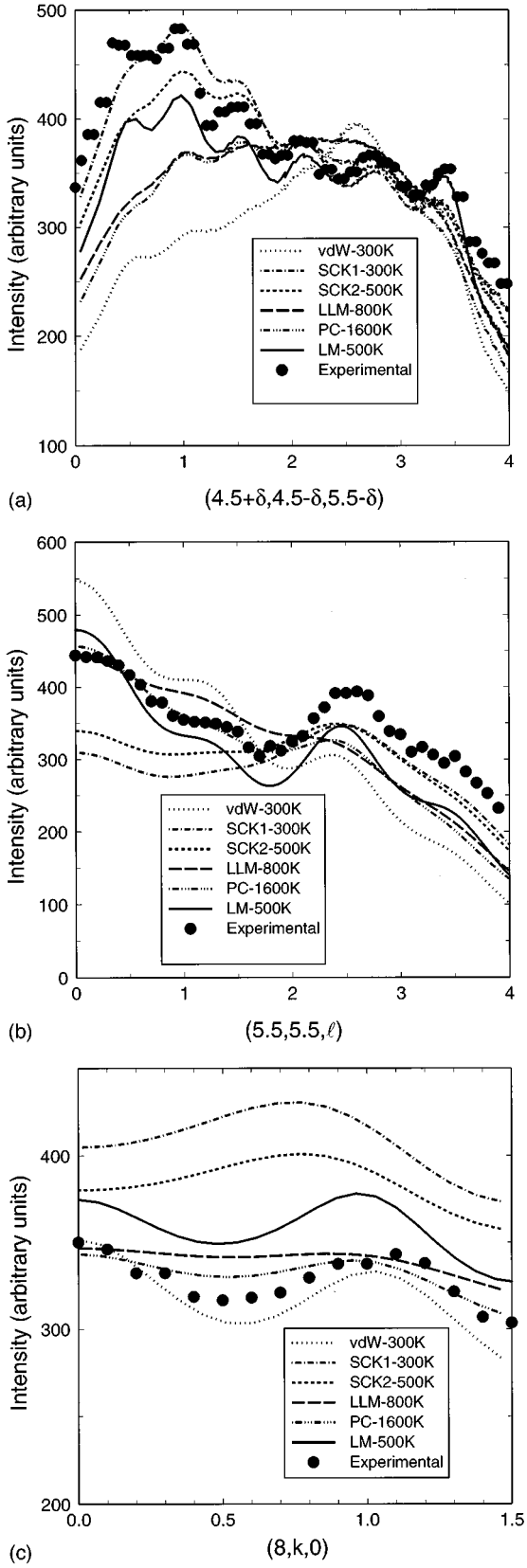

FIG. 4. Calculated intensities (up to a model dependent multiplication factor: 124 for vdW; 140 for SCK1, SCK2, and LLM; 130 for PC; and 125 for LM): (a) from (4.5,4.5,5.5) to (8.5,0.5,1.5), in the plane $h+k=9$, (b) from (5.5,5.5,0) to (5.5,5.5,4), in the plane $h+k=11$, (c) in the [8,k,0] direction. The observed intensities (Fig. 2) are shown for comparison.

$[1,-1,\pm 1]$ and $[0,0,1]$ directions in Figs. 1(a) and 1(b). The existence of diffuse streaks is also supported by the calculations as shown in Fig. 3(b) for the LM model, close to the mean-field transition temperature, where narrow $[1,-1,\pm 1]$ and $[0,0,1]$ streaks are visible. Hence, the diffuse scattering in C_{60} is possibly even more complicated than described previously in Ref. 6. It may combine 3D correlations, producing the X, L, and Γ scatterings, 2D correlations, in relation with the line scattering, and 1D correlations, possibly related to the H-shaped scattering, located in the $h+k=11$ plane. Complementary simulations to those presented here, namely, molecular dynamics or Monte Carlo ones, which give access to the arrangements of molecules,[7] could be very helpful to clarify this point.

VI. DISCUSSION

A. Existence of competing instabilities

Within the formalism of the symmetry-adapted functions used in this paper, all physical quantities—pair correlation functions, interaction, or susceptibility matrices—are developed over angular momenta l and irreducible representations τ of the space group $Fm\bar{3}m$ ($l=0,6,10,12$; $\tau=A_{1g},A_{2g},E_g,T_{1g},T_{2g}$). The diffuse intensity is expressed in terms of rotator pair correlation functions, proportional to the mean-field susceptibility components [Eqs. (6) and (21)]. All the 59×59 pair correlation, or $[\chi(\mathbf{q})]$, components contribute to the diffuse intensity. Indeed, in Ref. 6, we showed that calculations restricted to the $T_{2g}^{(3)}, l=10$ pair correlation function—considered as dominant in previous studies[27,28]—do not allow one to reproduce correctly the diffuse scattering, and the same is true if only some of the 59 rotators are taken into account (we checked this, for instance, for all the T_{2g} ones). Note, however, that the eigenvectors of the susceptibility associated with its highest eigenvalues contribute more (especially if they have strong $l=10$ components, since $l=10$ terms are reinforced in the expression of the diffuse intensity by the molecular form factor g_{10}).

Eigenvalues of the susceptibility $[\chi(\mathbf{q})]$ are plotted in Fig. 5, for the vdW and LM models, along some particular reciprocal space directions. Maxima at X, L, and Γ points are evidenced, which explain the corresponding diffuse scattering maxima. The related eigenvectors present definite symmetries. For instance, the eigenvectors associated with the highest eigenvalues at point X have only T_g (T_{1g} and T_{2g}) components, for both the vdW and LM models. A second order transition associated with the divergence of these eigenvalues would lead to a low temperature phase, the symmetry of which is related to the eigenvector symmetry; the $Pa\bar{3}$ phase is related to the divergence of the T_g representation at point X.[36] The part of the X point diffuse scattering coming from these eigenvectors can thus be associated with pretransitional fluctuations of the low temperature $Pa\bar{3}$ phase. Similar reasonings apply to all eigenvalues and eigenvectors of the susceptibility. Consequently, the X, L, and Γ point diffuse scattering can be associated with pretransitional fluctuations relative to competing phases, only one being stabilized below $T_0\simeq 260$ K: the $Pa\bar{3}$ phase. The same conclusion can be reached for the SCK, LLM, and PC models, for which the susceptibility eigenvalues also present maxima at points X, L, and Γ. A splitting of the heat-capacity anomaly around T_0 has been observed recently, which may correspond to an intermediate ordered phase between the $Fm\bar{3}m$ and $Pa\bar{3}$ ones;[38] this would corroborate our interpretation of the diffuse scattering results in terms of competing fluctuations.

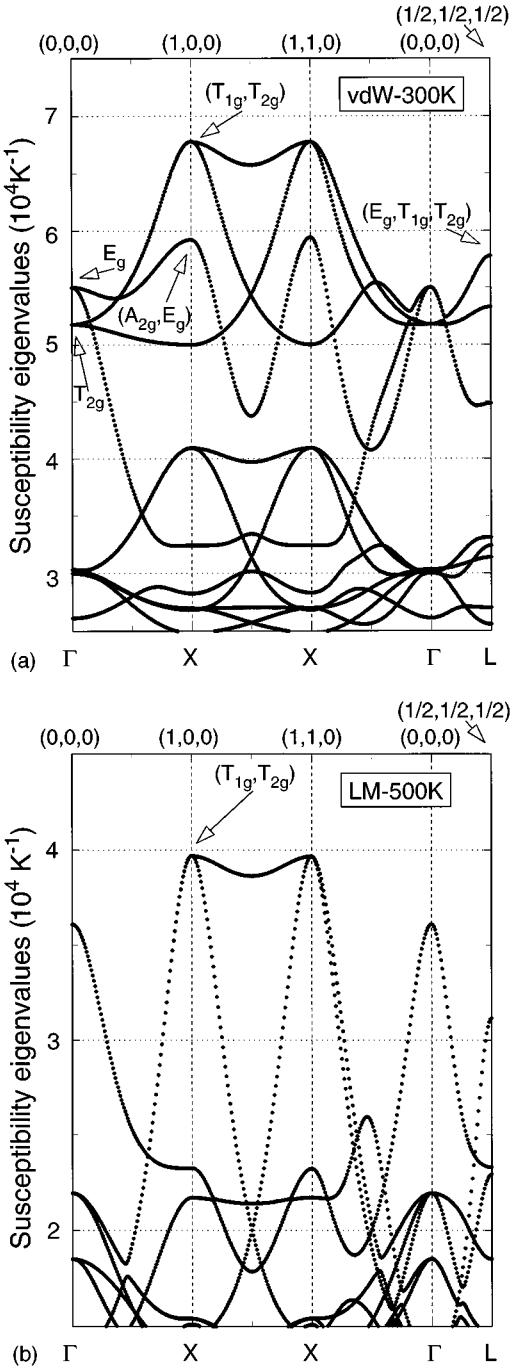

FIG. 5. Upper part of the eigenvalue spectrum of the susceptibility $[\chi(\mathbf{q})]$ along some reciprocal space directions, (a) for the vdW model, at $T=300$ K; (b) for the LM model, at $T=500$ K. Irreducible representations associated with some eigenvectors are indicated, to illustrate the existence of competing instabilities.

The existence of several competing instabilities in C_{60} stems from the high symmetry of this large molecule, combined with van der Waals or electrostatic interactions, only a function of the distances between interaction centers. This produces various relative orientational configurations be-

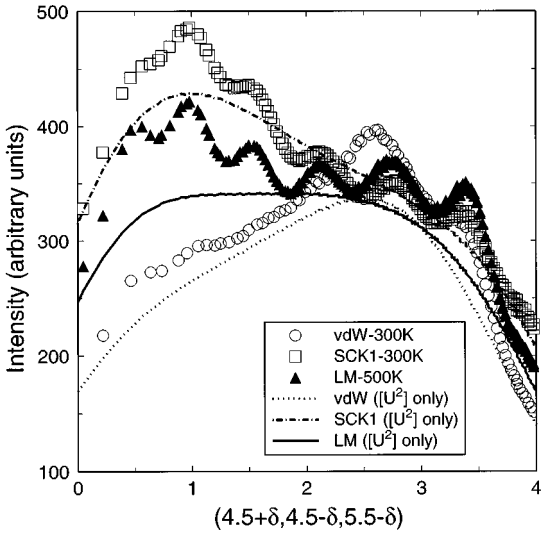

FIG. 6. Calculated diffuse intensity from (4.5,4.5,5.5) to (8.5,0.5,1.5), in the plane $h+k=9$, for the vdW, SCK1, and LM models. Calculations are made with and without ($[U^2]$ only) the $[J(\mathbf{q})]$ contribution.

tween neighboring molecules with nearly degenerate energies. The fluctuations associated with these different configurations contribute to the complexity of the diffuse scattering.

B. Role of the $[U^2]$ and $[J(\mathbf{q})]$ terms

1. Slow and rapid diffuse scattering modulations

In Sec. IV, the diffuse scattering intensity is expressed as a function of quantities directly related to the intermolecular interactions: the $[U^2]$ and $[J(\mathbf{q})]$ matrices. These have in fact somewhat distinct contributions to the diffuse intensity.[39] Schematically, the $[U^2]$ term—related to the average orientation of *one* molecule — gives slowly varying modulations of the diffuse halo, extending over several BZs, while the $[J(\mathbf{q})]$ term — related to correlations *between* molecules—gives more rapid variations of the diffuse scattering inside each BZ.[22] If $[J(\mathbf{q})]$ is set to zero, i.e., with $[U^2]$ only, the diffuse intensity varies slowly in reciprocal space; introducing $[J(\mathbf{q})]$ results in ''rapid'' modulations of this slowly varying scattering, as illustrated in Fig. 6.

For the vdW model, the calculated diffuse intensity is much too weak at the top of the plane $h+k=9$ [left parts of the scans in Figs. 4(a) or 6], while for the SCK1 model, it is much too weak at the center of the plane [Fig. 3(b) in Ref. 22]. Note in Fig. 6 and in Ref. 22 in Fig. 3(b) that these discrepancies are already present in the slowly varying part—$[U^2]$ component—of the scattering. Note also that the LM model yields the most convenient $[U^2]$ component, when the comparison with the observed diffuse scattering is performed in extended regions of reciprocal space, as motivated in Sec. V B. This is a reason why the LM model is the most satisfactory. Hence, an adequate $[U^2]$ matrix appears as a prerequisite to simulate the diffuse scattering in C_{60}. The $[U^2]$ terms corresponding to single molecule rotators averaged over the orientational mean-field energy [Eqs. (18) and (14)], the prerequisite concerns in fact the orientational mean-field energy.

2. High temperature mean-field energy

The orientational mean-field energy can be determined directly from Bragg peak intensity analysis, which gives access to single molecule properties. Equation (5) allows one to obtain the mean values of the A_{1g} rotators from the Bragg peak intensities. This was done by Schiebel *et al.*,[29] Chow *et al.*,[31] and David *et al.*,[32] for single crystal[29,31] and powder[32] samples, using x-rays[29,31] or neutrons.[29,32] One can then determine the orientational density distribution:[3,29]

$$f(\omega)=\sum_{l=0}^{\infty}\sum_{\tau=(A_{1g},\mu)}\frac{2l+1}{8\pi^2}\langle U_l^{\tau}(\omega)\rangle U_l^{\tau}(\omega), \qquad (25)$$

and thus the single-molecule mean-field energy, up to a constant term:[29]

$$E_{\mathrm{MF}}(\omega)=-kT\ln(f(\omega)). \qquad (26)$$

The mean-field energies deduced from Refs. 29,31 and 32 are reported in Fig. 7(a), for the rotation of the molecule about one of its sixfold axes in coincidence with a crystal threefold axis (the constant terms are arbitrarily chosen so that the absolute minima of the mean-field energies in Fig. 7 are zero). The mean-field energies present two minima, a primary one for the molecule with pentagons directed towards nearest neighbors (pentagon orientation) and a secondary one for hexagons towards nearest neighbors (hexagon orientation); note that in the high temperature phase the pentagons and hexagons do not necessarily face the nearest-neighbor double bonds. The minima or barrier height values differ only slightly for Chow *et al.* or Schiebel *et al.*, but a little more for David *et al.* This may be due to the fact that powder experiments are less accurate than single crystal ones, and/or to different temperatures for the experiments (room temperature for Chow and Schiebel, but 270 K for David). However, the results are in rather good agreement. Note also that the mean-field energy results confirm the validity of restricting the calculations to multipoles $l\leqslant 12$, as is shown in Fig. 7(b): the $l=12$ terms are indeed needed for the primary and secondary minima to be reproduced,[14] while the $l=16$ and 18 ones only induce relatively minor changes comparable to the scattering of the experimental results of Fig. 7(a). Using the above experimental mean-field energies obtained from certain studies,[29,31,32] we have calculated the $[U^2]$ matrices. The corresponding slowly varying scattering (multiplied by a scaling factor of 125) is drawn in Figs. 2(a)–2(c) for the neutrons (II) results[29] (very similar results are obtained from all the studies). A comparison with the observed diffuse scattering reveals that the slowly varying—or $[U^2]$— component extracted from Bragg peak analyses provides a fairly good ''background'' for the diffuse scattering intensity, further modulated, at the BZ scale, by the $[J(\mathbf{q})]$ intermolecular correlations.

We now turn to the mean-field energies calculated by solving the mean-field equations for the different models of intermolecular interactions [Fig. 8(a)]. They are normalized with respect to temperature since the physical quantity of interest is E_{MF}/T [see, e.g., Eq. (14)]. Most of the calculated mean-field energies are inconsistent with the experimentally determined ones. For the vdW, LLM, and PC models, the primary and secondary minima are the hexagon and pentagon orientations, respectively, instead of the pentagon and hexagon orientations. For the SCK models, the *P* and *H*

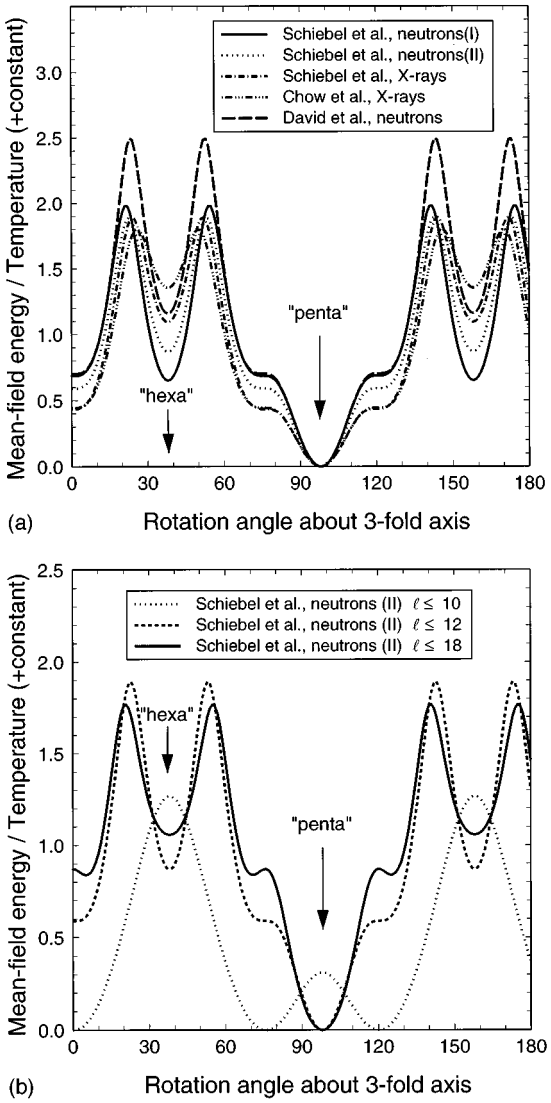

FIG. 7. (a) Mean-field energy normalized to the temperature as a function of the rotation angle about a threefold crystal axis, a molecular sixfold axis being aligned with this threefold crystal axis; from Eqs. (25) and (26), for $l \leqslant 12$, and from the results of the crystallographic studies of Schiebel *et al.* (Ref. 29) [three studies on three single crystals: neutrons (I), neutrons (II), and x-rays], Chow *et al.* (Ref. 31) (one single crystal, x-rays), and David *et al.* (Ref. 32) (powder sample, neutrons). Temperatures were, respectively, 295 K, 300 K, and 270 K. (b) Mean-field energy for neutrons (II) results, for $l \leqslant 10$, $l \leqslant 12$, and $l \leqslant 18$.

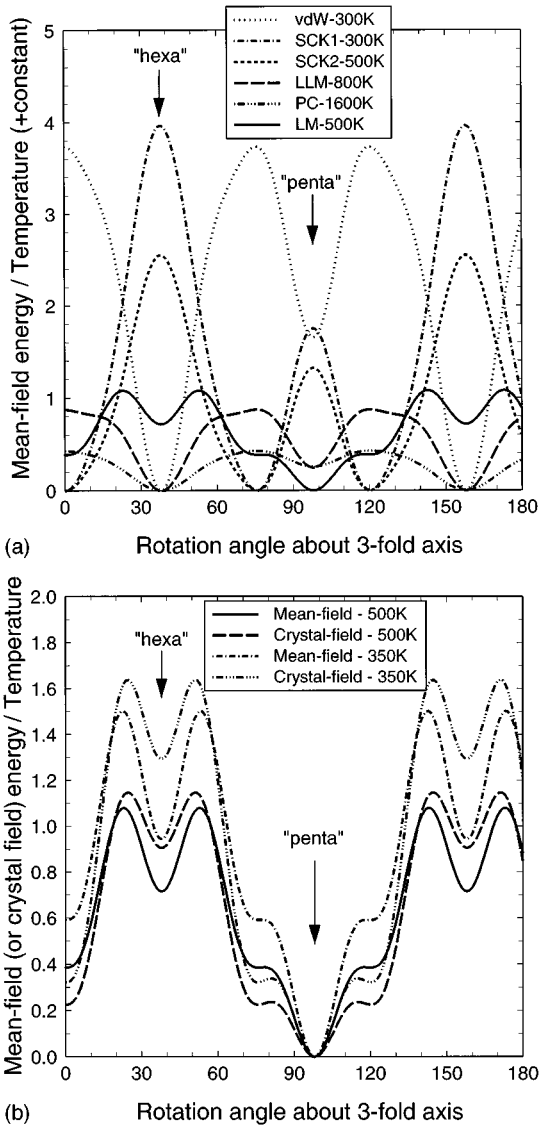

FIG. 8. (a) Mean-field energies normalized to the temperatures of calculations (Table II) as a function of the rotation angle about a threefold crystal axis, a sixfold molecular axis being aligned with this threefold crystal axis. They are calculated for all models in Table I, and for $l \leqslant 12$ [Eq. (12)]. (b) Mean-field and crystal-field energies for the LM model, at 350 K and 500 K, for $l \leqslant 12$ [Eq. (12) and (27)].

orientations are maxima instead of minima. Accordingly, for the above models, the slowly varying part of the diffuse scattering does not present the right variations, as already shown in Sec. VI B 1 for the vdW and SCK1 models [Fig. 6, and, in Ref. 22, Fig. 3(b)]. The only model which correctly predicts the true primary and secondary energy minima is the LM model, and correspondingly it is the one for which the slowly varying part of the diffuse scattering is the most adequate [compare Figs. 6 and 2(a)]. Actually, the LM model was worked out in order to fit the experimental Bragg peak data.[14,15,28] However, note that the LM model provides a satisfactory mean-field energy using a temperature of 350 K [Fig. 8(b)], close to that of Refs. 14 and 15, while the agreement with the ''experimental'' energy shown in Fig. 7(a) is not as good (the barrier height is too small) for $T=500$ K, which is on the other hand a more convenient temperature for simulating the diffuse scattering, as indicated in Sec. V A.

Let us now discuss the mean-field versus crystal-field approximations. The crystal-field energy is obtained by making a cruder approximation than for the mean-field one: all neighboring molecules are considered as spherical, which means that only their zero angular momentum is taken into account. Equations (12) and (13) become

$$E_{\mathrm{CF}}(\omega_i)=\sum_{l\geqslant 6,\tau} e_{l,\mathrm{CF}}^{A_{1g},\mu} U_l^{A_{1g},\mu}(\omega_i), \tag{27}$$

with

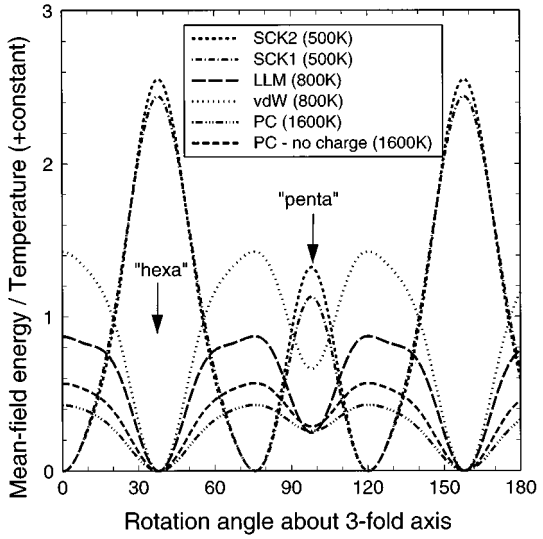

FIG. 9. Mean-field energies normalized to temperatures, as a function of the rotation angle about a threefold crystal axis, a sixfold molecular axis being aligned with this threefold crystal axis. These energies are calculated for all models with electrostatic charges in Table I, LLM, SCK2, and PC, and for the corresponding models without charges, at the same temperatures: vdW ($T=800$ K), SCK1 ($T=500$ K), and PC without charges ($T=1600$ K).

$$e_{l,CF}^{A_{1g},\mu}=12\times J_{l,l'=0}^{A_{1g},\mu;A_{1g}}(i,j) \tag{28}$$

(j refers to any of the twelve nearest-neighbor molecules of i: the interaction matrix terms $A_{1g}-A_{1g}$ are the same for all of them). Lamoen and Michel used this crystal-field approximation to refine their model of potential, but suggested that it would be interesting to perform the mean-field calculations, solving the self-consistent equations, i.e., taking into account the nonspherical components of the molecular density. Mean-field and crystal-field energies for the LM model are compared in Fig. 8(b). One finds that solving the self-consistent mean-field equations only leads to renormalizations of the crystal-field energies: the mean-field and crystal-field energy main characteristics and orders of magnitude are the same.

3. Role of electrostatic charges

The influence of adding electrostatic interactions to a given model can be understood from the previous discussion. For charge densities which do not overlap between neighboring molecules—this is the case in all models of Table I—the crystal-field energy is unchanged, due to the global neutrality of the molecule[14,15] [the $l'=0$ form factor relative to the electrostatic charge distribution being zero, the electrostatic $J_{l,l'=0}^{A_{1g},\mu;A_{1g}}$ terms are null in Eq. (28)]. The mean-field energy, which is rather similar to the crystal-field one, does not change much when adding charges. This is shown in Fig. 9 for the SCK2, LLM, and PC models and for the corresponding models with zero charges. For the sake of simplicity, we have not discussed the charge model of Burgos *et al.*[13] because its crystal-field energy is inconsistent with the ones determined experimentally (for instance, its primary and secondary minima are the hexagon and pentagon orientations, respectively). Adding electrostatic charges modifies the diffuse scattering: (i) the transition temperature is changed, and thus the calculation temperature and the relative weights of the $[U^2]$ and $[J(\mathbf{q})]$ matrices in the susceptibility, for instance; (ii) the matrix $[J(\mathbf{q})]$ is modified, now including also electrostatic interactions. Nonetheless, introducing (nonoverlapping) electrostatic charges cannot significantly modify the slowly varying part of the diffuse scattering—the $[U^2]$ component—which strengthens the previous argument in Sec. VI B 1 that a correct mean-field energy is mandatory.

C. Remarks on possible improvements of the models of interactions

As discussed above, the LM model[14,15] fits the best experimental diffuse scattering in the plastic phase $Fm\bar{3}m$. This is because it has been elaborated on the criterion of the mean-field energy, i.e., of correct $A_{1g}-A_{1g}$ interaction terms, but it does not insure that other interaction terms, in the $[J]$ matrix, are adequate. Comparison of the diffuse scattering data and of its slowly varying part (experimental $[U^2]$ term) in Fig. 2(a) shows that the contribution of the $[J(\mathbf{q})]$ terms must be large in the upper (and lower) parts of the plane $h+k=9$ [left side of Fig. 2(a)]. It appears that this contribution is not sufficiently pronounced for the LM model [see Figs. 4(a) and 6]. It may indicate that the LM model does not fully account for the intermolecular interactions in C_{60}.

Further improvements of the models could be obtained using the C_{60} low temperature properties which should also be reproduced satisfactorily. The properties we consider here are the following (see, e.g., Ref. 3 and references therein): (i) the low temperature energy presents nearly degenerate minima in the P and H configurations, the lower for the P configuration, energy differences being ≈ 11 meV; (ii) the barrier height between them is of about 250 meV, but can reach 500 meV for a threefold axis rotation depending on which assumptions are made from the experimental data (the 250 meV barrier may correspond to a twofold axis rotation); (iii) the absolute values of energy minima should be of about -1.7 eV (cohesive energy[24]). These energies were (at least partly) determined from single molecule reorientation analyses, and thus should be tested using the potential energy of a single rotating molecule. However, the P and H configurations being both present in the $Pa\bar{3}$ phase, there can be various molecular environments. Still, the potential energy should not strongly depend on them, at least for points (i) and (iii), because of the near degeneracy between the P and H configurations. Figure 10 shows the potential energy, in the $Pa\bar{3}$ phase, of a molecule rotating about its local threefold axis with its twelve neighbors in P orientations. None of the models of interactions in Table I satisfies the three above criteria (see also Refs. 3,12,19,24 and 41–43). Table III shows that (i) energy differences between P and H configurations are too important, (ii) the barrier height is too small for the vdW and SCK models, and (iii) the absolute value of energy minimum is too small for the LM model.

Our calculations of the high temperature diffuse scattering, together with the supplementary low temperature constraints, clearly show that the physical or chemical arguments (representation of multiple bonds by analogy with solid nitrogen,[11] explicit differentiation between σ and π

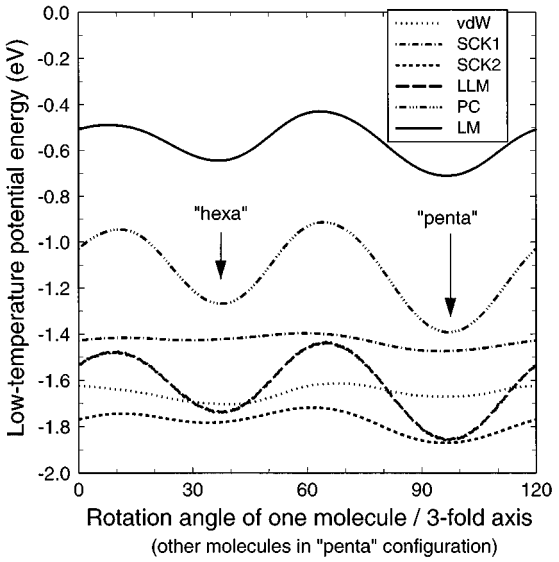

FIG. 10. Energy in the low temperature phase $Pa\bar{3}$, for all the models in Table I; calculations are performed for domain *A* following the notation of Ref. 40 and they are restricted to nearest-neighbor interactions; a central molecule is rotated about its local threefold axis, its twelve neighbors being in *P* orientations.

bondings,[14,15] tetrahedron bonding,[17] etc.) used to build models for the interactions are still partly inadequate. Some additional ingredients are needed, which could come from *ab initio* calculations of the electronic structure of the molecule.[28] Such calculations were done by Yildirim, Harris, Erwin, and Pederson.[19] At first,[19] they neglected the charge density overlap between neighboring molecules, which leads to small Coulomb interactions between C_{60} molecules, smaller than in Refs. 11 and 12, for instance. This result motivated Lamoen and Michel to work mainly on improving the description of the van der Waals–like interactions.[15] However, Yildirim[44] extended the calculations in Ref. 19 and found that the small overlapping between charge densities of neighboring molecules is not negligible. On this basis, Savin, Harris, and Yildirim[24] have very recently elaborated a model of potential which, considering the preceding discussions about low temperature properties, looks very promising. The charge overlaps should ensure a more important role to the electrostatic interactions, with respect to the diffuse scattering (the mean-field energy will now depend on electrostatic interactions, arguments in Sec. VI B 3 applying only to nonoverlapping charges); the role of van der Waals–type and electrostatic interactions is more equilibrated. Test of the model of Savin, Harris, and Yildirim, based on diffuse scattering analyses, appears as highly desirable and will thus be the subject of forthcoming investigations.

VII. CONCLUSION

In this paper, a detailed analysis of room temperature single crystal x-ray diffuse scattering data was presented. Diffuse scattering calculations were performed starting from microscopic models of intermolecular interactions,[10–12,15,17] using a mean-field theory and the formalism of the symmetry-adapted functions. The preliminary analysis presented in Ref. 22 for the vdW and SCK1 models[10,11] has been extended to most of the current models of interactions. This provides an overview of their relative worths with regard to the diffuse scattering. We have shown that the analysis of the diffuse scattering is a good probe for the intermolecular interactions in C_{60} (which should of course be combined with tests on the other available structural, dynamical, and energetical properties).

Our main results are the following:

(i) A prerequisite for any model to correctly fit the diffuse scattering is to give the right mean-field energy. If not, additional electrostatic charges will not allow one to improve sufficiently the calculated diffuse scattering (unless significant overlap is considered[24]).

(ii) All models of interactions account for the basic features of the diffuse scattering (X,L,Γ point plus extra scatterings). But none of them, even the best one with regard to diffuse scattering—the LM model[15]—is fully adequate when comparison with experimental data is made over large regions in reciprocal space.

(iii) The very complex diffuse scattering in C_{60} is due to the existence of pretransitional competing fluctuations. This is related to the fact that the C_{60} molecule is a large and highly symmetrical molecule.

The need for more physical and/or chemical constraints to understand these interactions is emphasized. In this respect, a very recent model,[24] based on electrostatic charge distribution determined from *ab initio* calculations,[19] is promising.

TABLE III. Low temperature energy characteristics from experiments (cf. Refs. 3 and 24 for instance) and for the different models of intermolecular interactions of Table I. The calculated values are obtained for a single molecule rotating about its local threefold axis, with all its neighbors in *P* orientation (cf. Fig. 10; note that the *H* orientation is not a true minimum for the SCK1 model).

	Energy difference between *P* and *H* orientations (meV)	Barrier height from *P* to *H* orientation (eV)	Energy minimum (eV)
Experiments	−11	0.25−0.5	−1.7
vdW	+34	∼0.09	∼−1.7
SCK1	−53	∼0.08	∼−1.5
SCK2	−87	∼0.15	∼−1.9
LLM	−120	∼0.42	∼−1.9
LM	−66	∼0.28	∼−0.7
PC	−123	∼0.48	∼−1.4

ACKNOWLEDGMENTS

We wish to acknowledge S. Savin, K.H. Michel, and J.R.D. Copley for communicating their results prior to publication, and for very interesting discussions. We are also indebted to L. Pintschovius, K. Parlinski, and W. Prandl for fruitful conversations. This work is based on experimental data made possible by the high quality and large size of the C_{60} single crystals skillfully grown by J.M. Godard.

*Electronic address: launois@lps.u-psud.fr, sylvain@csd.uwm.edu, moret@lps.u-psud.fr

[1] H.W. Kroto, J.R. Heath, S.C. O'Brien, R.F. Curl, and R.E. Smalley, Nature (London) **318**, 162 (1985).

[2] W. Kratschmer, L.D. Lamb, K. Fortiropoulos, and D.R. Huffman, Nature (London) **347**, 354 (1990).

[3] J.D. Axe, S.C. Moss, and D.A. Neumann, in *Solid State Physics: Advances in Research and Applications*, edited by H.E. Ehrenreich and F. Spaepen (Academic Press, New York, 1994), Vol. 48, pp. 149–224.

[4] R. Moret, S. Ravy, and J.M. Godard, J. Phys. (France) I **2**, 1699 (1992); **3**, 1085 (1993).

[5] O. Blaschko, R. Glas, Ch. Maier, M. Haluska, and H. Kuzmany, Phys. Rev. B **48**, 14 638 (1993).

[6] P. Launois, S. Ravy, and R. Moret, Phys. Rev. B **52**, 5414 (1995).

[7] L. Pintschovius, S.L. Chaplot, G. Roth, and G. Heger, Phys. Rev. Lett. **75**, 2843 (1995).

[8] P. Wochner *et al.* (unpublished).

[9] Y. Guo, N. Karasawa, and W.A. Goddard III, Nature **351**, 464 (1991).

[10] A. Cheng and M.L. Klein, J. Phys. Chem. **95**, 6750 (1991); Phys. Rev. B **45**, 1889 (1992).

[11] M. Sprik, A. Cheng, and M.L. Klein, J. Phys. Chem. **96**, 2027 (1992).

[12] J.P. Lu, X.-P. Li, and R.M. Martin, Phys. Rev. Lett. **68**, 1551 (1992); X.-P. Li, J.P. Lu, and R.M. Martin, Phys. Rev. B **46**, 4301 (1992).

[13] E. Burgos, E. Halac, and H. Bonadeo, Phys. Rev. B **47**, 13 903 (1993); **49**, 15 544 (1994).

[14] D. Lamoen and K.H. Michel, Z. Phys. B **92**, 323 (1993).

[15] D. Lamoen and K.H. Michel, J. Chem. Phys. **101**, 1435 (1994).

[16] K.H. Michel and J.R.D. Copley,in *Fullerens and Fullerene Nanostructures*, edited by H. Kuzmany, M. Mehring, and S. Roth (World Scientific, Singapore, 1996), pp. 381–384.

[17] L. Pintschovius and S.L. Chaplot, Z. Phys. B **98**, 527 (1995).

[18] R. Heid, Phys. Rev. B **47**, 15 912 (1993).

[19] T. Yildirim, A.B. Harris, S.C. Erwin, and M.R. Pederson, Phys. Rev. B **48**, 1888 (1993).

[20] T.R. Welberry and B.D. Butler, J. Appl. Crystallogr. **27**, 205 (1994); Chem. Rev. **95**, 2369 (1995).

[21] J.R.D. Copley, D.A. Neumann, R.L. Capelletti, and W.A. Kamitakahara, J. Phys. Chem. Solids **53**, 1353 (1992).

[22] S. Ravy, P. Launois, and R. Moret, Phys. Rev. B **53**, 10 532 (1996); Phys. Rev. B **xx**, xx (1996).

[23] R. Moret, P. Launois, and S. Ravy, Fullerene Sci. Technol. (to be published).

[24] S. Savin, A.B. Harris, and T. Yildirim (unpublished).

[25] Molecular dynamics simulations presented in Ref. 7 took several hundred hours of CPU time on a parallel computer. Our mean-field calculations are performed on a HP735 work-station. The main part of the calculations is the preliminary computation of all the elements of the interaction matrix J (see Sec. IV), which takes a few tens of hours; calculation of the diffuse intensity in any reciprocal plane takes only a few minutes, typically.

[26] See, e.g., H.M. James and T.A. Keenan, J. Chem. Phys. **31**, 12 (1959); W. Press and A. Hüller, Acta Crystallogr. A **29**, 252 (1973); W. Press, *ibid.* **29**, 257 (1973); **32**, 170 (1976); A. Hüller and W. Press, *ibid.* **35**, 876 (1979); K. H. Michel and K. Parlinski, Phys. Rev. B **31**, 1823 (1985); R.M. Lynden-Bell and K.H. Michel, Rev. Mod. Phys. **66**, 721 (1994).

[27] K.H. Michel, J.R.D. Copley, and D.A. Neumann, Phys. Rev. Lett. **68**, 2929 (1992).

[28] J.R.D. Copley and K.H. Michel, J. Phys. Condens. Matter **5**, 4353 (1993).

[29] P. Schiebel, K. Wulf, W. Prandl, G. Heger, R. Papoular, and W. Paulus, Acta Crystallogr. A **52**, 176 (1996).

[30] K.H. Michel, D. Lamoen, and W.I.F. David, Acta Crystallogr. A **51**, 365 (1995).

[31] P.C. Chow, X. Jiang, G. Reiter, P. Wochner, S.C. Moss, J.D. Axe, J.C. Hanson, R.K. McMullan, R.L. Meng, and C.W. Chu, Phys. Rev. Lett. **69**, 2943 (1992).

[32] W.I.F. David, R.M. Ibberson, and T. Matsuo, Proc. R. Soc. London Ser. A **442**, 129 (1993). Rotator mean values given in this paper have to be corrected by a factor $1/\sqrt{2}$ (Ref. 30).

[33] W. Prandl, P. Schiebel, and K. Wulf, Acta Crystallogr. A **52**, 171 (1996).

[34] C.J. Bradley and A.P. Cracknell, *The Mathematical Theory of Symmetry in Solids* (Clarendon, Oxford, 1972).

[35] Formula (24) was given by Heid (Ref. 18) for electrostatic or van der Waals interactions, varying as $1/r^n$. Extension of this formula to Buckingham, Born-Mayer potentials (Refs. 15 and 17) with an exponential term may be justified by a development of $\exp(-Cr)$ over inverse powers of r.

[36] The fact that a given model can predict a second order phase transition towards the true $Pa\bar{3}$ phase is in favor of this model (Ref. 24). However, taking into account the first order character of the transition, it may happen that the stable low temperature phase is not the one corresponding to the divergence of a susceptibility eigenvalue. One should solve the mean-field equations and calculate the free energies for different possible low temperature phases, as a function of temperature, in order to determine the most stable ones. In the case of the vdW model where we find that the highest eigenvalues are of T_g symmetry [$Pa\bar{3}$ phase (Refs. 18 and 37)], it turns out that the first phase stabilized at low temperature is the tetragonal phase $P4_2/mnm$ (Ref. 18).

[37] H.T. Stockes and D.M. Hatch, *Isotropy Subgroups of the 230 Crystallographic Space Groups* (World Scientific, Singapore, 1988).

[38] J.E. Fischer, A.R. McGhie, J.K. Estrada, M. Haluska, H. Kuzmany, and H.-U. ter Meer, Phys. Rev. B **53**, 11 418 (1996).

[39] In the following, the contributions of the $[U^2]$ and $[J(\mathbf{q})]$ matrices to the diffuse scattering intensity are presented as distinct, which is a simplification since such a decoupling cannot be done mathematically in Eq. (22). Moreover, one should remember that these matrices are both determined from the same model of intermolecular interactions. However, the above simplification allows one to understand interesting features of the calculations, which are themselves performed rigorously from Eq. (22).

[40] A.B. Harris and R. Sachidanandam, Phys. Rev. B **46**, 4944 (1992).
[41] T. Yildirim and A.B. Harris, Phys. Rev. B **46**, 7878 (1992).
[42] J. Yu, L. Bi, R.K. Kalia, and P. Vashishta, Phys. Rev. B **49**, 5008 (1994).
[43] J.Q. You, T. Xie, and B.Y. Yang, Phys. Rev. B **51**, 1358 (1995).
[44] T. Yildirim, in *International Winterschool on Electronic Properties of Novel Materials*, edited by H. Kuzmany, J. Fink, M. Mehring, and S. Roth (World Scientific, Singapore, 1994), pp. 162–166.